Journal of Sound and Vibration (2002) **255**(4), 685–700
doi:10.1006/jsvi.2001.4184, available online at http://www.idealibrary.com on IDEAL®

ACTIVE–PASSIVE PIEZOELECTRIC ABSORBERS FOR SYSTEMS UNDER MULTIPLE NON-STATIONARY HARMONIC EXCITATIONS

R. A. MORGAN AND K. W. WANG

Structural Dynamics and Controls Laboratory, Department of Mechanical and Nuclear Engineering, The Pennsylvania State University, University Park, PA 16802-1412, *U.S.A.*

(*Received* 28 *March* 2001, *and in final form* 3 *December* 2001)

Previous research has shown that piezoelectric materials can be shunted with electrical networks to form devices that operate similarly to a mechanical vibration absorber. These systems can be tuned to provide modal damping (modal tuning) or to attenuate a harmonic disturbance (tonal tuning). Semi-active piezoelectric absorbers have also been proposed for suppressing harmonic excitations with varying frequency, a scenario that cannot be easily controlled using passive devices. However, these semi-active systems have limitations that restrict their applications. In a previous study, the authors have developed a high performance active–passive alternative to the semi-active absorber that uses a combination of a passive electrical circuit and active control actions. The active control consists of three parts: an *adaptive inductor tuning action*, a *negative resistance action*, and a *coupling enhancement action*. This new device has been shown, both analytically and experimentally, to be very effective for the suppression of harmonic disturbances with time-varying frequency. In the present paper, the adaptive active–passive piezoelectric absorber configuration is extended so that it can track and suppress multiple harmonic excitations. A new optimal tuning law is derived, and the stability conditions of the system are investigated. The effectiveness of this new multi-frequency absorber design is demonstrated by comparing its performance and control power requirement to the popular Filtered-x adaptive feedforward control algorithm.

1. INTRODUCTION

Piezoelectric materials have been shown to be useful for passive vibration damping and absorption. Shunting the piezoelectric material with a circuit containing resistive and inductive elements creates an electro-mechanical vibration damper/absorber [1]. These devices can be tuned to suppress a harmonic excitation at a given frequency (tonal tuning). The principal drawback of tonally tuned absorbers is that they require the absorber damping to be very low to achieve good performance, which causes the effective bandwidth to be quite small [2]. For this reason, passive absorbers are not generally useful in off-resonance situations, especially when the excitation frequency is unsteady or varying.

In recent years, semi-active piezoelectric absorber designs have been proposed to suppress harmonic excitations with time-varying frequency. The implementation of these semi-active absorbers requires either a variable inductor or a variable capacitor element, where both of these methods have some inherent limitations. For instance, the variable capacitor method [3] limits the tuning of the piezoelectric absorber to a relatively small frequency range. The variable inductor approach [4], which is accomplished using

0022-460X/02/$35.00

a synthetic inductance circuit, can add a significant parasitic resistance to the circuit, which is generally undesirable for narrow-band applications. In addition, these semi-active implementations have had difficulty in achieving fast and accurate tuning. In a previous study, the authors have introduced a high performance adaptive active–passive piezoelectric absorber as an alternative to these semi-active absorbers [5]. The fundamental concept behind this new absorber design is the integration of a fixed passive inductance with an active variable inductance, which allows fast and accurate frequency tuning while minimizing the required control power. In addition, negative resistance and active coupling enhancement actions were added to the control law to significantly improve the performance and robustness of the absorber, compared to a passive or semi-active piezoelectric absorber. This design combines the advantages of active and passive systems, which are high performance and increased efficiency, with the adaptability of a semi-active absorber. The configuration used here is similar to the previously developed active–passive piezoelectric network (APPN) system [6], but the problem of interest and the control algorithm are considerably different here.

One of the drawbacks of this new active–passive absorber, as well as the semi-active absorbers that have been proposed in the past, is that they are only able to suppress a single harmonic excitation. Since disturbance sources with multiple varying frequencies do occur in many real world applications, the objective of this research is to expand the active–passive absorber concept to address the multiple frequency issue. In addition to a new passive circuit design, new control laws and a modified optimal tuning law are derived. The stability conditions for the multi-frequency absorber system are also derived using Lyapunov's method. Finally, the effectiveness of the new configuration is demonstrated by comparison to a state-of-the-art adaptive feedforward control law.

2. MULTI-FREQUENCY PIEZOELECTRIC ABSORBER CONFIGURATION

A schematic of the system under consideration is illustrated in Figure 1, which consists of a piezoelectric actuator and sensor integrated into a general mechanical structure. The sensor provides feedback to an external voltage source that is in series with an electrical circuit. It is assumed that the system model can be obtained, either analytically or experimentally, in the form

$$M\underline{\ddot{q}} + C\underline{\dot{q}} + K^D\underline{q} + K_C Q = \underline{\hat{F}}\cdot f(t), \qquad V_a = \frac{1}{C_p^S} Q + K_C^{\mathrm{T}}\underline{q}. \tag{1}$$

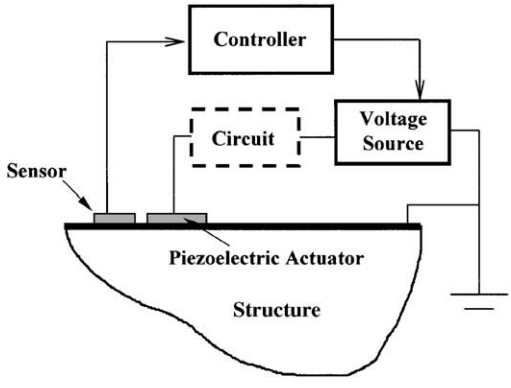

Figure 1. General system configuration.

The matrices M, C and K^D are the mass, damping, and open-circuit stiffness matrices of the system, q is a vector of the generalized co-ordinates of the structure, and Q is the charge on the piezoelectric. The vector K_c represents the coupling between the mechanical and electrical systems, $f(t)$ is the excitation force, and the vector $\hat{F}$ contains the weightings of the excitation force on the individual structural co-ordinates. V_a is the voltage across the piezoelectric actuator, which is used to integrate the circuit equation into the system model. For the single-frequency piezoelectric absorber, a series R–L circuit is used and the resulting circuit equation can be written as

$$L\ddot{Q} + R\dot{Q} + \frac{1}{C_p^S}Q + K_C^{\mathrm{T}}\underline{q} = V_C. \tag{2}$$

We begin by considering some multi-frequency circuit designs for passive piezoelectric vibration absorbers that have been previously developed. One possible approach is to add R–L–C circuits in parallel with the original R–L shunt circuit; thus, introducing additional resonances that can be tuned to other frequencies [7]. The shortcoming of this approach is that the dynamics of the individual circuit branches are strongly coupled, so a numerical optimization routine is needed to determine the circuit parameters that will achieve the desired tunings. For this reason, this approach is not applicable to an adaptive piezoelectric absorber. Another approach is to introduce resonant L–C blocking filters to effectively decouple the individual circuit branches [8]. A schematic for a two-mode passive piezoelectric absorber using this approach is given in Figure 2.

The purpose of this circuit, as originally proposed, is to provide modal damping around the resonant frequencies ω_1 and ω_2, where it is assumed that $\omega_1 < \omega_2$. The parallel combination of L_{21} and C_{21} has a resonant frequency, which is tuned to ω_1. The subscript 21 denotes the blocking filter in branch 2 that is tuned to ω_1. The decoupling effect of this blocking filter can be seen in the electrical impedances of the circuit branches, as shown in Figure 3. Note that the impedance of branch 1 is higher than branch 2 (without the blocking filter) because the lower frequency ω_1 requires a larger inductance L_1. For frequencies near ω_1, most of the current from the piezoelectric material would flow into the second branch, causing the first branch to be ineffective. The purpose of the blocking filter is to increase the impedance of the second circuit branch for frequencies near ω_1. At these frequencies, the second branch acts like an open circuit due to the large impedance of the blocking filter, which causes the first branch to function like a single-frequency absorber. The blocking filter is, in general, not necessary for the second branch of the circuit to function because the

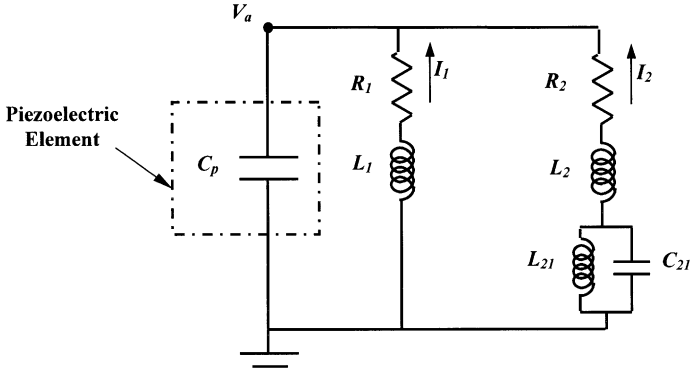

Figure 2. Two-mode passive piezoelectric absorber [8].

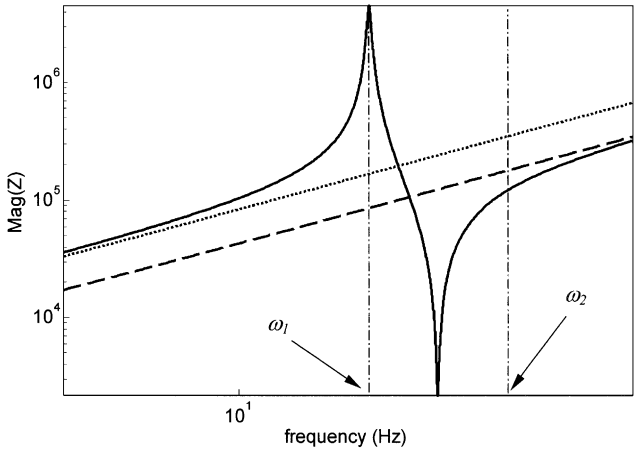

Figure 3. Circuit branch electrical impedances. Branch 1 (·····), Branch 2 without blocking filter (------), Branch 2 (——). ($C_{21} = C_p^s$, $\omega_1 = 20$ Hz, $\omega_2 = 40$ Hz, $\zeta_i = 0{\cdot}02$, $\zeta_{21} = 0{\cdot}0005$.

impedance of the higher frequency branch is already significantly lower than that of the first branch [8]. Ideally, we would like the blocking filter to have very little effect on the impedance of the second branch for frequencies near ω_2. Although the impedance of the blocking filter must be sufficiently large to provide the decoupling effect that enables the first branch to function, a large blocking impedance can have a significant effect on the second circuit branch as well. For example, in Figure 3 it can be seen that at the frequency ω_2 the impedance of the second branch with blocking filter is slightly lower than that of the original circuit consisting only of R_2 and L_2. Physically, this means that the blocking filter impedance is partially cancelling the impedance of the inductance L_2, which can decrease the effectiveness of the second branch. The effects of the blocking filter impedance on the performance of the multi-frequency absorber will be further considered in section 3.

Using the configuration shown in Figure 2 as a starting point, the concept is modified so that it can be applied to an adaptive active–passive piezoelectric absorber design. First, we would like to be able to independently vary the tuning of each circuit branch. This requires the use of separate control inputs for each circuit branch. Secondly, we cannot use a passive L–C blocking filter if the circuit natural frequencies are changing. For the first branch to be effectively decoupled from the second, the resonant frequency of the blocking filter must always be tuned to ω_1. This problem can be overcome by actively implementing an adaptive blocking filter. Thus, the circuit design for the active–passive multi-frequency piezoelectric absorber reduces to the configuration shown in Figure 4.

The passive inductances L_{1p} and L_{2p} are used to tune the circuit to be resonant at the nominal or steady state excitation frequencies. We begin designing the control law for the multi-frequency adaptive absorber by incorporating the same three components as the single-frequency case [5]. The first part of the control law is designed to imitate a variable inductor so that the absorber can be adaptively tuned to the correct frequency. The advantages of the active inductor include fast and accurate adjustment, no parasitic resistance, and easier implementation compared to a semi-active inductor. No passive resistance is intentionally added to the shunt circuit; however, the passive inductors will contain some internal resistances, which are denoted R_{1p} and R_{2p}. If these internal resistances are excessively large, the narrow-band disturbance rejection performance of the absorber is degraded. In this case, an active negative resistance action is used to reduce the effective resistances in the absorber circuit. Finally, the effective coupling in the circuit

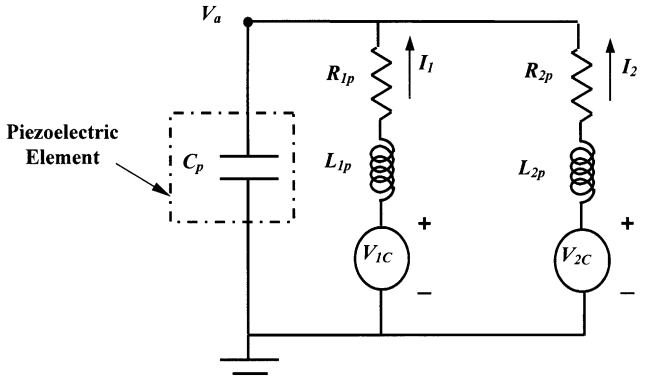

Figure 4. Active–passive multi-frequency piezoelectric absorber configuration.

equation is enhanced by using the third part of the control law, which is the active coupling enhancement action. This action significantly improves the performance and robustness of the absorber.

The control law for the first circuit branch, which is shown in equation (3), is identical to that of the single-frequency piezoelectric absorber, where L_{1a} is the active variable inductance, R_{1a} is the negative resistance, and G_{ac} is the active coupling gain. In addition to these three elements, the control input for the second branch must also provide the voltage for the adaptive blocking filter. To calculate this voltage, the impedance of the blocking filter (in the Laplace domain) is first expressed as shown in equation (4). The damping term ζ_{21} has been added to the original L–C design to improve the stability of the blocking filter. The resulting control voltage for the second branch of the circuit is given in equation (5).

$$V_{1C} = -L_{1a}(t)\cdot \dot{I}_1 + R_{1a}I_1 - (G_{ac} - 1)K_C^{\mathrm{T}}q, \tag{3}$$

$$Z_{21}(s) = \frac{-V_{21}}{I_2} = \frac{\beta_{21}}{C_p^s}\frac{s + 2\zeta_{21}\omega_1}{s^2 + 2\zeta_{21}\omega_1 s + \omega_1^2}, \quad \text{where } \beta_{21} = \frac{C_p^s}{C_{21}}, \tag{4}$$

$$V_{2C} = -L_{2a}(t)\cdot \dot{I}_2 + R_{2a}I_2 - (G_{ac} - 1)K_C^{\mathrm{T}}q + V_{21}(t). \tag{5}$$

3. OPTIMAL TUNING FOR MULTI-FREQUENCY PIEZOELECTRIC ABSORBER

To ensure that the active inductance is properly tuned, an expression for the optimal tuning on a general multiple-degree-of-freedom (MDOF) structure is derived. The tuning ratio δ_i is defined in equation (6), where ω_{ia} is the ith circuit frequency and ω_{ie} is the estimate of the ith excitation frequency. The frequency estimates are obtained on-line using an algorithm based on the recursive least-squares method [9]. This algorithm has proven to have excellent convergence speed and is quite insensitive to noise. The required input is a sensor signal that is dominated by the harmonic excitation.

$$\delta_i = \frac{\omega_{ia}}{\omega_{ie}} \quad \text{where } \omega_{ia} = \frac{1}{\sqrt{(L_{ip} + L_{ia})C_p^S}}. \tag{6}$$

To begin the derivation of the optimal tuning law, the system model is first transformed into modal space using the transformation $q = U\eta$, where U is a matrix containing the eigenvectors of the structure model. The displacement of the structure at a desired point is chosen as the objective function, which is then expressed as a weighted sum of the modal responses, as shown in equation (7), where W is the modal weighting vector. The optimal tuning ratio for the single-frequency absorber is given in terms of the system modal parameters by equation (8), where ω_n is a vector of the modal frequencies of the structure. The $\sim$ notation denotes the system parameters after transformation to the modal space, and the subscripts i and j denote the ith and jth elements of a vector.

$$w_d(t) = W^{\mathrm{T}}\eta(t), \tag{7}$$

$$\delta_{opt} = \left[1 + G_{ac} C_p^S \frac{\sum_{j=1}^{n} W_j M_j (a_j - \tilde{F}_j b)}{\sum_{j=1}^{n} W_j M_j \tilde{F}_j} \right]^{-1/2}, \tag{8}$$

where

$$M_j = \frac{1}{\omega_{n_j}^2 - \omega_e^2}, \quad a_j = \tilde{K}_{c_j} \sum_{i=1}^{n} \frac{\tilde{K}_{c_i} \tilde{F}_i}{\omega_{n_i}^2 - \omega_e^2}, \quad b = \sum_{i=1}^{n} \frac{\tilde{K}_{c_i}^2}{\omega_{n_i}^2 - \omega_e^2}.$$

The key assumptions in this derivation are that the excitation frequency is changing relatively slowly compared to the system dynamics (quasi-steady state) and that the structural and circuit damping can be neglected.

The main challenge in the design of the multi-frequency absorber is determining the optimal tunings for each branch of the circuit. As in the single-frequency case, we would like to find an expression for the optimal tuning ratio in terms of the modal parameters of the system. Recall that the blocking filter configuration was chosen to facilitate the determination of the optimal circuit tunings. While the decoupling effect of the blocking filter is indeed helpful in this respect, the dynamics of the blocking filter can also cause the optimal circuit tunings for the multi-frequency absorber to be considerably different from those of the corresponding single frequency absorbers.

We begin by considering the optimal tuning of the first circuit branch for the excitation frequency ω_1. Since the blocking filter 21 is resonant at this frequency, the second branch acts like an open circuit because of the large impedance. For this reason, the first branch can be treated as a single-frequency absorber, and equation (8) can be used to solve for the optimal tuning ratio $(\delta_1)_{opt}$. Next, we consider the optimal tuning of the second branch for the given excitation frequencies ω_1 and ω_2. There are two reasons that the optimal branch inductance L_2 is dependent on ω_1. First, the blocking filter contains a capacitance as well as a variable inductance that depends on ω_1, which changes the effective inductance in the second branch of the circuit. Secondly, the first circuit branch and the blocking filter both add additional dynamics to the system. These additional modes can have a significant effect on the optimal tuning ratio δ_2, just like higher order structural modes. These problems can be solved by lumping the known circuit dynamics with the structural model, as shown in equation (9). This augmented system model treats the states Q_1 and Q_{21}, which are defined as the integrals of the currents in the inductors L_1 and L_{21}, as structural co-ordinates. Note that the augmented system is in the same form as equations (1) and (2), except that the damping terms are absent and the effective capacitance

is different.

$$\underbrace{\begin{bmatrix} M & 0 & 0 \\ 0 & G_{ac}L_1 & 0 \\ 0 & 0 & \dfrac{G_{ac}\beta_{21}}{\omega_1^2 C_p^S} \end{bmatrix}}_{M_2} \underbrace{\begin{Bmatrix} \ddot{q} \\ \dfrac{1}{G_{ac}}\ddot{Q}_1 \\ \dfrac{1}{G_{ac}}\ddot{Q}_{21} \end{Bmatrix}}_{\ddot{q}_2} + \underbrace{\begin{bmatrix} K^D & G_{ac}K_C & 0 \\ G_{ac}K_C^{\mathrm{T}} & \dfrac{G_{ac}}{C_p^S} & 0 \\ 0 & 0 & \dfrac{G_{ac}\beta_{21}}{C_p^S} \end{bmatrix}}_{K_2} \underbrace{\begin{Bmatrix} q \\ \dfrac{1}{G_{ac}}Q_1 \\ \dfrac{1}{G_{ac}}Q_{21} \end{Bmatrix}}_{q_2} + \underbrace{\begin{bmatrix} K_C \\ \dfrac{1}{C_p^S} \\ \dfrac{-\beta_{21}}{C_p^S} \end{bmatrix}}_{K_{C2}} Q_2 = \underbrace{\begin{bmatrix} \hat{F} \\ 0 \\ 0 \end{bmatrix}}_{\hat{F}_2} f(t), \tag{9}$$

$$L_2\ddot{Q}_2 + \underbrace{\frac{1+\beta_{21}}{C_p^S}}_{1/C_{p2}^S} Q_2 + G_{ac}\underbrace{\begin{bmatrix} K_C^{\mathrm{T}} & \dfrac{1}{C_p^S} & \dfrac{-\beta_{21}}{C_p^S} \end{bmatrix}}_{K_{C2}^{\mathrm{T}}} q_2 = 0.$$

The previously derived optimal tuning law (equation (8)) can now be applied to this augmented system model. First, the augmented system model is transformed to modal space using the mass-normalized eigenvector matrix, as shown in equation (10). The modal frequencies of the augmented system ω_{n2} are obtained from the solution of the eigenvalue problem, and the remaining parameters needed to use the optimal tuning law are given in equation (11).

$$q_2 = U_2\eta_2, \quad \text{where } K_2U_2 = M_2U_2[\omega_{n2}^2] \text{ and } U_2^{\mathrm{T}}M_2U_2 = 1, \tag{10}$$

$$\tilde{K}_c = U_2^{\mathrm{T}}K_{C2}, \qquad \tilde{F} = U_2^{\mathrm{T}}\hat{F}_2, \qquad C_{p2}^S = \frac{C_p^S}{1+\beta_{21}}. \tag{11}$$

We will now examine a typical optimal tuning curve predicted by the procedure specified above. First, we must introduce the example system used to generate these results. The system used throughout this study is a cantilevered beam with a collocated piezoelectric actuator and sensor pair attached near the root of the beam. The parameters of the example system are given in Table 1. In all subsequent results, the response of interest is the tip displacement of the beam.

In some situations, the optimal tuning law for the multi-frequency piezoelectric absorber gives results that are similar to the single-frequency absorber. If the frequency ratio

TABLE 1

System parameters

Length of beam	196 mm
Thickness of beam	3·2 mm
Width of beam and piezos	25·4 mm
Distance from root of beam to piezos	9·5 mm
Length of piezos	58·8 mm
Thickness of piezos	0·5 mm
Piezoelectric constant (d_{31})	−175e−12 m/V
Modulus of piezos ($1/s_{11}^E$)	65 GPa
Dielectric constant of piezos ($\varepsilon_{33}^{\mathrm{T}}$)	1·5e−8 F/m
Generalized coupling coeff. (K_{31})	0·141

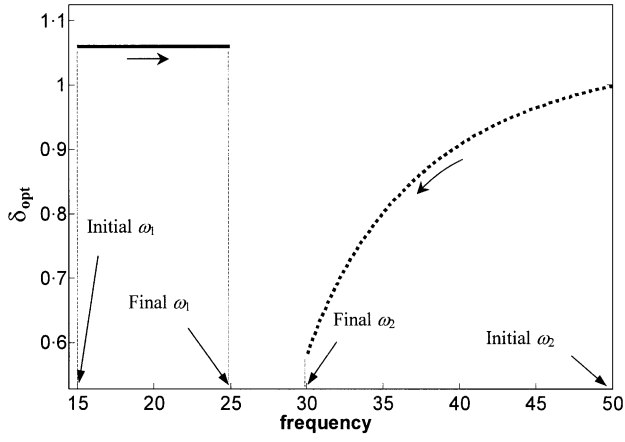

Figure 5. Example optimal tuning curves. Optimal δ_1 (——), optimal δ_2 (· · · ·). ($\omega_{10} = 20$ Hz, $\omega_{20} = 40$ Hz, $\Delta_1 = \Delta_2 = 0{\cdot}25$, $\dot{\omega}_1/\omega_{10} = 0{\cdot}02$, $\dot{\omega}_2/\omega_{20} = -0{\cdot}02$, $G_{ac} = 14$).

$r = \omega_2/\omega_1$ is relatively constant, the optimal tuning ratios will be only slightly frequency dependent, much like in the single-frequency absorber case. However, a varying frequency ratio can cause the optimal tuning ratio for the second branch to be strongly frequency dependent, as shown in Figure 5. In the case shown here, both excitation frequencies are changing at a normalized rate of $|\dot{\omega}/\omega_0| = 0{\cdot}02$ (the rate of change is 2% of the nominal excitation frequency per second) but ω_1 is increasing while ω_2 is decreasing. Because the excitation frequencies are moving in opposite directions, the frequency ratio r decreases from 3·33 to 1·2 in this case, which causes the optimal tuning ratio δ_2 to decrease sharply.

This phenomenon can be explained qualitatively by considering the impedance matching criterion, which states that the impedance of the multi-frequency circuit should be matched to that of a single-frequency absorber (R_2 and L_2 only) at the frequency ω_2 [8]. As the frequency ratio r approaches unity, the impedance of the blocking filter at ω_2 approaches negative infinity. To counteract this and allow the impedance matching condition to be satisfied, the inductance L_2 must become infinitely large, which causes the optimal tuning ratio δ_2 to approach zero. Although the impedance matching criterion can be used to explain some of the trends shown in Figure 5, it neglects the effects of the additional electrical dynamics and higher order structural modes on the optimal tuning ratios. The results shown in Figure 5 are generated using the optimal tuning procedure outlined above, which gives more accurate results than the impedance matching criteria since it takes into account all of the dynamics of the system.

Note that the use of only one blocking filter provides decoupling of the two circuit branches only at the frequency ω_1. This partial decoupling is sufficient to allow the optimal tuning ratios to be solved sequentially, as described above. We originally assumed that the circuit branches are partially decoupled at the frequency ω_2 because the impedance of the lower frequency branch should be significantly higher due to the larger inductance L_1. This assumption is invalid when the frequencies are close together ($r \approx 1$) because the impedances of the two branches will be similar in magnitude. However, because the dynamics of the first branch are included when solving for the optimal tuning ratio δ_2, the above procedure still provides very accurate tuning in these situations.

Next, we examine the steady state performance of the multi-frequency piezoelectric absorber and consider the effect of the parameter β_{21}, which is essentially the gain

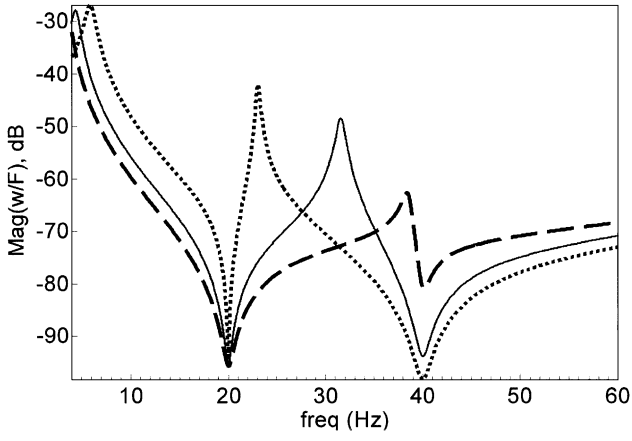

Figure 6. Steady state performance comparison. $\beta_{21} = 0{\cdot}12$ (·····), $\beta_{21} = 1$ (——), $\beta_{21} = 10$ (- - - - -). ($\omega_{10} = 20$ Hz, $\omega_{20} = 40$ Hz, $G_{ac} = 14$, $\zeta_i = 0{\cdot}02$, $\zeta_{21} = 0{\cdot}0005$).

parameter for the adaptive blocking filter. The steady state frequency responses of the system for several different values of β_{21} are shown in Figure 6. As discussed earlier in section 3, there is a compromise in the performance at the two excitation frequencies that depends on how large the impedance of the blocking filter is. Note that for the $\beta_{21} = 1$ case the response notches produced at ω_1 and ω_2 are approximately equal in size. For large values of β_{21} (larger blocking filter impedances), the decoupling action of the blocking filter is more effective so the performance is increased slightly near ω_1. However, this excessively large impedance of the blocking filter also degrades the performance near ω_2 considerably. For smaller values of β_{21} (smaller blocking filter impedances), the decoupling action becomes less effective, which decreases the performance near ω_1 but increases the performance at ω_2 slightly. If our goal is to produce equally large notches at both excitation frequencies, then $\beta_{21} = 1$ appears to be the best in this case. However, it will be shown in section 5 that the optimal selection of β_{21} for transient excitation suppression may be considerably different than these steady state results suggest.

These steady state results also show that the active coupling gain causes the performance to be quite robust with respect to frequency variations even without using the adaptive tuning mechanism—either excitation frequency can vary as much as 15% from nominal (for the $\beta_{21} = 1$ case) and the performance will still be better than the original system (without the absorber). Without the active coupling gain, however, the performance can be worse than the original system for even a 2% change from the nominal frequency, unless the adaptive tuning is used to compensate for this frequency change. A general observation is that when the excitation frequency is changing even slightly, the active tuning action is extremely helpful in achieving maximum performance. This is true even in the case where a large active coupling gain is used to increase the robustness of the absorber, since the vibration attenuation provided by a fixed-frequency absorber decreases rapidly as the excitation frequency varies from nominal.

4. STABILITY ANALYSIS FOR MULTI-FREQUENCY PIEZOELECTRIC ABSORBER

In a previous study [5], the stability criteria for the single-frequency adaptive piezoelectric absorber were derived using Lyapunov's method. A similar analysis is now

performed for the multi-frequency absorber. The total system energy is selected to be the Lyapunov function candidate. The system mass, damping and stiffness matrices are derived similarly to those shown in equation (9), except that the state Q_{21} is replaced by the voltage across the blocking filter (V_{b2}), which eliminates the need for the coupling vector in the system equation. In order to simplify the derivation of the Lyapunov stability criteria, it is desired that the system mass and stiffness matrices be symmetric. Initially, these matrices are not symmetric, but they can be made symmetric by applying the co-ordinate transformations shown in equation (12), where the overbar denotes the new (transformed) co-ordinates. The resulting system equation is shown in equation (14). The Lyapunov function candidate is then expressed in terms of the transformed system model, as shown in equation (13). Next, the sufficient conditions under which these system mass and stiffness matrices are positive definite are derived, so that equation (13) is indeed a valid Lyapunov function.

$$q = \frac{1}{G_{ac}}\bar{q}, \quad Q_1 = \bar{Q}_1, \quad Q_2 = (1+\beta_{21})\bar{Q}_2 + \frac{C_p^S}{\beta_{21}L_2}\bar{V}_{b2}, \quad V_{b2} = \frac{1}{\omega_1^2}\bar{V}_{b2}, \tag{12}$$

$$V(\bar{z}) = \bar{z}^{\mathrm{T}} K_{sys}\bar{z} + \dot{\bar{z}}^{\mathrm{T}} M_{sys}\dot{\bar{z}}, \tag{13}$$

$$\underbrace{\begin{bmatrix} \frac{1}{G_{ac}}M & 0 & 0 & 0 \\ 0 & L_1 & 0 & 0 \\ 0 & 0 & (1+\beta_{21})L_2 & \frac{C_p^S}{\beta_{21}} \\ 0 & 0 & \frac{C_p^S}{\beta_{21}} & \frac{1}{L_2}+\frac{1}{\omega_1^2} \end{bmatrix}}_{M_{sys}} \underbrace{\begin{Bmatrix} \ddot{\bar{q}} \\ \ddot{\bar{Q}}_1 \\ \ddot{\bar{Q}}_2 \\ \ddot{\bar{V}}_{b2} \end{Bmatrix}}_{\ddot{\bar{z}}} + \underbrace{\begin{bmatrix} \frac{1}{G_{ac}}C & 0 & 0 & 0 \\ 0 & R_1 & 0 & 0 \\ 0 & 0 & (1+\beta_{21})R_2 & \frac{R_2 C_p^S}{L_2\beta_{21}} \\ 0 & 0 & \frac{2\zeta_{21}\omega_1}{C_p^S}\beta_{21}(1+\beta_{21}) & 2\zeta_{21}\omega_1\left(\frac{1}{L_2}+\frac{1}{\omega_1^2}\right) \end{bmatrix}}_{C_{sys}} \underbrace{\begin{Bmatrix} \dot{\bar{q}} \\ \dot{\bar{Q}}_1 \\ \dot{\bar{Q}}_2 \\ \dot{\bar{V}}_{b2} \end{Bmatrix}}_{\dot{\bar{z}}}$$

$$+ \underbrace{\begin{bmatrix} \frac{1}{G_{ac}}K^D & K_C & K_C & 0 \\ K_C^{\mathrm{T}} & C_p^S & C_p^S & 0 \\ K_C^{\mathrm{T}} & C_p^S & \frac{1+\beta_{21}}{C_p^S} & 0 \\ 0 & 0 & 0 & 1 \end{bmatrix}}_{K_{sys}} \underbrace{\begin{Bmatrix} \bar{q} \\ \bar{Q}_1 \\ \bar{Q}_2 \\ \bar{V}_{b2} \end{Bmatrix}}_{\bar{z}} = 0. \tag{14}$$

The condition that results from requiring K_{sys} to be positive definite is

$$\left| \frac{1}{G_{ac}}K^D - C_p^S K_C K_C^{\mathrm{T}} \right| > 0 \tag{15}$$

This condition, which gives an upper bound on the active coupling gain, is identical to the one obtained in the stability analysis of the single-frequency piezoelectric absorber. As discussed in the previous study [5], it can be shown that this condition is a necessary condition for stability as well. It was also shown that in the case of a SDOF system, the

maximum active coupling gain can be expressed quite simply in terms of K_{ij}, the generalized coupling coefficient of the system [1].

Having found the conditions under which the Lyapunov function candidate is valid, we now consider its time derivative, which is

$$\dot{V}(\bar{z}) = -\dot{\bar{z}}^{\mathrm{T}}(\underbrace{C_{sys} - \tfrac{1}{2}\dot{M}_{sys}}_{C_{eff}})\dot{\bar{z}} + \tfrac{1}{2}\,\bar{z}^{\mathrm{T}}\dot{K}_{sys}\bar{z}. \tag{16}$$

With the co-ordinate transformation that was chosen above, the time-derivative of the system stiffness matrix K_{sys} is identically zero, which greatly simplifies the Lyapunov stability criteria. The time-derivative of $V(\bar{z})$ can then be said to be at least negative semi-definite if the matrix C_{eff} is positive semi-definite. The conditions under which this can be guaranteed are derived using Sylvester's criteria [10], and the results are shown in equations (17) and (18). Note that the effective resistances have been expressed in terms of the closed-loop damping ratios ζ_i, as shown in equation (19).

$$2\zeta_1\omega_1\delta_1 + \frac{\dot{\omega}_1}{\omega_1} \geqslant 0 \quad \text{and} \quad 2\zeta_2\omega_2\delta_2 + \frac{\dot{\omega}_2}{\omega_2} \geqslant 0, \tag{17}$$

$$\frac{L_2}{\omega_1^2}\left(2\zeta_2\omega_2\delta_2 + \frac{\dot{\omega}_2}{\omega_2}\right)\left(2\zeta_b\omega_1 + \frac{\dot{\omega}_1}{\omega_1}\right) + \frac{\dot{\omega}_2}{\omega_2}\left(2\zeta_b\omega_1 - 2\zeta_2\omega_2\delta_2 - \frac{\dot{\omega}_2}{\omega_2}\right) \geqslant 0, \tag{18}$$

$$R_i = R_{ip} - R_{ia} = \frac{2\zeta_i}{C_p^S\omega_{ia}}. \tag{19}$$

The closed-loop system can then be guaranteed to be stable if the conditions given in these equations, as well as equation (15), are satisfied. Note that the failure to meet these conditions does not imply instability, as Lyapunov's method only provides sufficient conditions for stability.

The first two conditions are similar to the previously derived stability condition for the single-frequency piezoelectric absorber in that they give a lower bound on the frequency rate of change [5]. By examining these conditions, it can be seen that they will not be violated unless the damping in the absorber circuit is excessively small and the excitation frequencies are decreasing very rapidly. The third and final stability condition, which is given in equation (18), also gives bounds on the frequency rates of change that are dependent on both the circuit damping and the damping the blocking filter. Except in the case where the damping terms are extremely small and the excitation frequencies are decreasing very rapidly, the first-half of the condition shown in equation (18) will be positive. The sign of the second term is primarily dependent on whether the second excitation frequency is increasing or decreasing, and on the relative magnitude of the terms containing the damping ratios for branch two and the blocking filter. This condition can then be used to safely select the damping quantities in the absorber design given the expected frequency change rates.

The above equations give the conditions under which the transformed system can be guaranteed to be stable. The definition of stability for non-autonomous systems states that for every $\varepsilon > 0$ and $t_0 \geqslant 0$ there exists a $\bar{\delta}(\varepsilon, t_0) > 0$ such that $\|\bar{z}(t_0)\| < \bar{\delta}$ implies $\|\bar{z}(t)\| < \varepsilon$ for every $t \geqslant t_0$ [11]. Since the coefficients of the linear co-ordinate transformation given in equation (12) are finite, we can always find a $\delta(\varepsilon, t_0) > 0$ such that $\|z(t_0)\| < \delta$ implies $\|z(t)\| < \varepsilon$ for every $t \geqslant t_0$. In other words, the only thing necessary to prove stability of the

original system from the above results is to choose a different bound on the initial conditions of the system. Note that the above Lyapunov stability analysis does not guarantee asymptotic stability, since the time-derivative of $V(\bar{z})$ is only negative semi-definite even when C_{eff} is positive definite. This is because $V(\bar{z}) = 0$ any time $\dot{\bar{z}} = 0$, even if $\bar{z} \neq 0$. However, it can be shown using La Salle's theorem that the above conditions do indeed guarantee asymptotic stability [11]. Notice from equation (16) that the only way in which the system can maintain the $\dot{V}(\bar{z}) = 0$ condition is if $\dot{\bar{z}} = \ddot{\bar{z}} = 0$. From the system equation (14), it can be seen that this is possible only when $\bar{z} = 0$. Thus for positive definite C_{eff}, $\dot{V}(\bar{z})$ is negative definite everywhere, except at the origin $\bar{z} = 0$, so the system is asymptotically stable. Proving asymptotic stability of the transformed system also proves it for the original system because $\bar{z} = 0$ implies that $z = 0$ as well (from equation (12)).

5. TRANSIENT PERFORMANCE OF MULTI-FREQUENCY ABSORBER

In this section, we evaluate the effectiveness of the multi-frequency adaptive piezoelectric absorber for suppressing harmonic excitations with time-varying frequencies. For the purpose of comparison, the filtered-x adaptive feedforward control law [12] is selected as a baseline. The filtered-x algorithm generates the control signals directly from the measured excitation using an adaptive discrete-time finite impulse response (FIR) filter with four coefficients (two coefficients are required for each harmonic excitation). This control law has been shown to be very effective for the suppression of harmonic disturbances with varying frequency. The excitation signal used in this section is a summation of two linear chirp signals, with nominal frequencies of $\omega_{10} = 20$ Hz and $\omega_{20} = 40$ Hz. The bandwidth of both chirp signals is fixed at $\Delta = 0{\cdot}05$, which means that the excitation frequencies increase linearly from $0{\cdot}95\omega_{10}$ to $1{\cdot}05\omega_{10}$ and from $0{\cdot}95\omega_{20}$ to $1{\cdot}05\omega_{20}$. The frequency rates of change are varied over a range of $\dot{\omega}/\omega_0 = 0{\cdot}005$ to $0{\cdot}05$. For a given bandwidth and frequency rate of change, the required time span can be calculated. The performance index used is the root-mean-square (r.m.s.) of the response at the point of interest. The control effort index is the r.m.s. control power, which is calculated using the apparent power (the product of the r.m.s. current and r.m.s. voltage) of the source.

We begin by fixing the adaptation gain α of the filtered-x controller [12, 5] and optimizing the parameters of the adaptive blocking filter for the active–passive absorber. For simplicity, the closed-loop damping ratios of the two circuit branches, represented by ζ_i, are selected to be equal. Figure 7 shows the r.m.s. response of the system with the active–passive absorber versus the parameters β_{21} and ζ_{21} for a moderately fast changing excitation case. The optimal blocking filter parameters for this case are $\beta_{21} = 0{\cdot}12$ and $\zeta_{21} = 0{\cdot}0005$. If we examine the control effort instead of the performance we find that these parameters also provide a near-minimum power requirement. Investigating faster and slower excitation cases shows that the optimal blocking filter parameters are also quite insensitive to the frequency rate of change. It is interesting to note that the optimal β_{21} for the transient excitation considered here is significantly lower than the β_{21} that appeared to be optimal from the steady state response shown in Figure 6. However, the steady state results did not take into account the transient dynamics of the blocking filter, which is a lightly damped resonant system. It is reasonable to expect that these transient dynamics could have a negative effect on the transient response of the system, and a larger value of β_{21} would amplify the blocking filter response at all frequencies.

Next, we examine the effects of the absorber damping ratio and the frequency rate of change on the performance of the multi-frequency piezoelectric absorber, as shown in Figure 8. This figure shows that the performance of the multi-frequency absorber is slightly

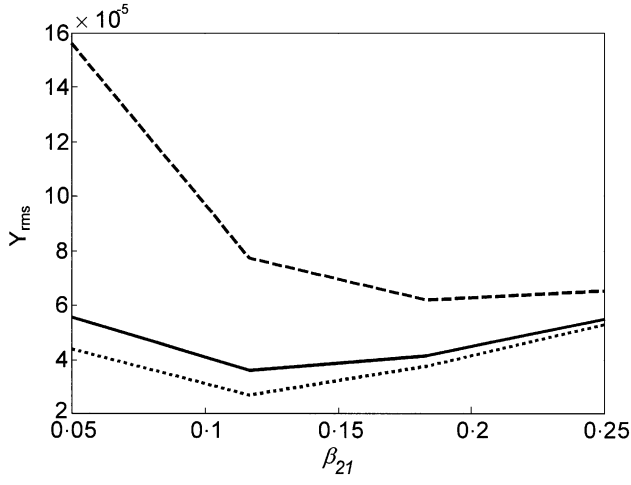

Figure 7. Performance effects of β_{21} and ζ_{21}. $\zeta_{21} = 0{\cdot}0005$ (·····), $\zeta_{21} = 0{\cdot}0006$ (——), $\zeta_{21} = 0{\cdot}02$ (- - - - -). ($\dot{\omega}/\omega_0 = 0{\cdot}0275$, $\zeta_i = 0{\cdot}2$, $G_{ac} = 14$).

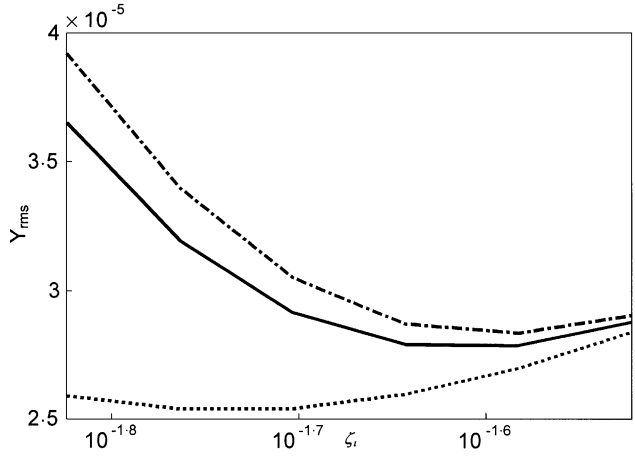

Figure 8. Performance effects of ζ_i and $\dot{\omega}$. $\dot{\omega}/\omega_0 = 0{\cdot}005$ (·····), $\dot{\omega}/\omega_0 = 0{\cdot}0275$ (——), $\dot{\omega}/\omega_0 = 0{\cdot}05$ (- · - · - · - · -). ($\zeta_{21} = 0{\cdot}0005$, $\beta_{21} = 0{\cdot}12$, $G_{ac} = 14$).

better for slowly changing excitations, although the performance loss for more rapidly changing excitations is not very large. The optimal absorber damping ratios obtained from this plot range from $\zeta_i = 0{\cdot}017$ for the slowest case to $\zeta_i = 0{\cdot}026$ for the fastest case. The parameter study on the effects of ζ_i also shows that the control power requirement of the active–passive multi-frequency absorber is affected very little by this parameter. For this reason, we select the "optimal" parameters for the multi-frequency absorber as the ones that provide the best performance.

Finally, we examine the relative performance and control effort of the optimized multi-frequency absorber compared to the multi-frequency filtered-x baseline system. The performance index is selected to be the per cent reduction in structural r.m.s. response of the active–passive absorber system compared to the filtered-x baseline. Similarly, the per cent reduction in r.m.s. control power is selected as an index of the control effort requirement. Since both the performance and the control effort of the baseline system are strongly

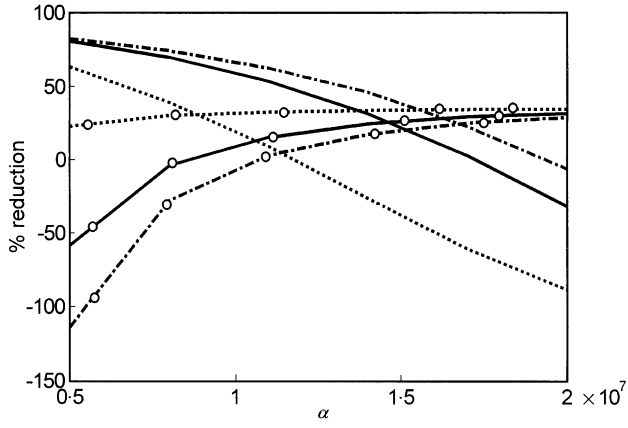

Figure 9. Relative performance ($Y_{r.m.s.}$) and control power ($(P_c)_{r.m.s.}$) comparison. $Y_{r.m.s.}$ for $\dot{\omega}/\omega_0 = 0{\cdot}005$ (·····), $Y_{r.m.s.}$ for $\dot{\omega}/\omega_0 = 0{\cdot}0275$ (——), $Y_{r.m.s.}$ for $\dot{\omega}/\omega_0 = 0{\cdot}05$ (-·-·-·-·-·-), $(P_c)_{r.m.s.}$ for $\dot{\omega}/\omega_0 = 0{\cdot}005$ (- - - -○- -○- - - -), $(P_c)_{r.m.s.}$ for $\dot{\omega}/\omega_0 = 0{\cdot}0275$ (—○—○—), $(P_c)_{r.m.s.}$ for $\dot{\omega}/\omega_0 = 0{\cdot}05$ (-·-·-·-○-·-·-·-). ($\zeta_1 = \zeta_{opt}$, $\zeta_{21} = 0{\cdot}0005$, $\beta_{21} = 0{\cdot}12$, $G_{ac} = 14$).

dependent on the adaptation gain α, we plot the results versus this gain, as shown in Figure 9. This figure shows a pair of lines representing the percent reduction in r.m.s. response and r.m.s. control power for each of the three excitation speeds considered. In each case, a range of α exists where the active–passive absorber outperforms the filtered-x baseline while requiring less control power (both per cent reductions indices are positive). The reverse situation, where the filtered-x baseline has better performance and less control power requirement (both indices are negative), does not occur. This is due to the compromise between the performance and control power requirement of the filtered-x controller. As was mentioned previously, this trade-off in the optimal design of the multi-frequency absorber is almost insignificant. This is most likely due to the active–passive nature of the piezoelectric absorber, which is inherently more energy efficient than a purely active system.

Figure 9 also shows that at high filtered-x gains the relative performance of the active–passive absorber decreases significantly while the relative control power requirement decreases only slightly. From these results, it would appear that the filtered-x controller is a better choice when high performance is required. However, evaluating only the relative performance can be somewhat misleading in this case. Compared to the short-circuit system, the active–passive absorber system shown above produces a 92% reduction in the structural r.m.s. response. At the highest gains shown in Figure 9, the filtered-x controller produces a 92–96% reduction in the r.m.s. response compared to the short-circuit system, with the largest reductions corresponding to the slowly changing excitation cases. Because both methods are so effective, the absolute performance gain produced by the larger filtered-x gains are actually quite insignificant. Thus, it can be said that the active–passive absorber design can achieve a better balance between performance and efficiency than the filtered-x method.

6. EXTENSION TO THREE OR MORE EXCITATION FREQUENCIES

To this point, we have restricted the analysis of the adaptive multi-frequency piezoelectric absorber to the dual-frequency example for simplicity. In practice, the methods and analysis

presented in sections 3 and 4 can be extended to higher order cases in a quite straightforward manner. Consider the circuit diagram shown in Figure 4. For the case where n excitation frequencies are to be suppressed by the absorber, the active–passive circuit must contain n branches, each containing a passive inductance and a control input. In addition, the ith circuit branch will include $i-1$ active blocking filters that are tuned to the excitation frequencies below ω_i. For example, the third branch in a triple frequency absorber configuration will contain two active blocking filters of the form shown in equation (4) with gains β_{31} and β_{32} and resonant frequencies ω_1 and ω_2. The general form of the control input for the ith branch is

$$V_{iC} = -L_{ia}(t)\cdot \dot{I}_i + R_{ia} I_i - (G_{ac} - 1) K_C^{\mathrm{T}} q + V_{ib}(t), \tag{20}$$

$$\text{where } V_{ib}(s) = -\left(\sum_{j=1}^{i-1} \frac{\beta_{ij}}{C_p^S} \frac{s + 2\zeta_{ij}\omega_j}{s^2 + 2\zeta_{ij}\omega_j s + \omega_j^2} \right) I_i(s).$$

The optimal tuning derivation for higher order piezoelectric absorbers can also be performed in a manner analogous to that shown in section 4. Once again, the optimal tuning ratios for each branch are solved successively starting with the lowest frequency branch and the known circuit dynamics are lumped together with the structure model. For branch i, the known circuit dynamics include the $i-1$ previous branch circuit equations as well as the $i-1$ active blocking filter equations contained in branch i. In principle, the Lyapunov stability analysis could also be extended to higher order absorber designs in a similar manner.

7. CONCLUSIONS

In this paper, a new multi-frequency adaptive piezoelectric vibration absorber design is presented. It uses a combination of a simple passive shunt circuit along with an adaptive active control law. The active control law enhances the passive piezoelectric absorber in four ways: it adds an adaptive tuning ability by imitating a variable inductance, it reduces the effective resistance in the absorber circuit to increase performance, it increases the effective coupling of the system to increase robustness and performance, and it effectively decouples the dynamics of the individual circuit branches. This decoupling action allows the tunings of the multi-frequency absorber to be calculated using an analytical optimal tuning law. The stability criteria of the multi-frequency piezoelectric absorber device are also derived.

The proposed design is shown to be effective for simultaneously suppressing two harmonic excitations with time-varying frequencies. For the purpose of comparison, the adaptive feedforward filtered-x algorithm is used as a baseline. It is shown that the multi-frequency adaptive piezoelectric absorber can achieve better performance while requiring less control power, compared to the filtered-x algorithm. The design and analysis presented here can also be extended in a straightforward manner to cases with three or more excitation frequencies.

ACKNOWLEDGMENTS

This research is sponsored by the U.S. Army Research Office with Dr. Gary Anderson as the project monitor.

REFERENCES

1. N. W. HAGOOD and A. H. VON FLOTOW 1991 *Journal of Sound and Vibration* **146**, 243–268. Damping of structural vibrations with piezoelectric materials and passive electrical networks.

2. A. H. VON FLOTOW, A. BEARD and D. BAILEY 1994 *Proceedings of NOISE-CON* 94 (*Ft. Lauderdale, FL*), 437–455. Adaptive tuned vibration absorbers: tuning laws, tracking agility, sizing, and physical implementations.
3. C. L. DAVIS and G. A. LESIEUTRE 2000 *Journal of Sound and Vibration* **232**, 601–617. An actively tuned solid-state vibration absorber using capacitive shunting of piezoelectric stiffness. doi: 10.1006/jsvi.1999.2755.
4. J. H. HOLLKAMP and T. F. STARCHVILLE JR 1994 *Journal of Intelligent Material Systems and Structures* **5**, 559–566. A self-tuning piezoelectric vibration absorber.
5. R. A. MORGAN and K. W. WANG 2000 *Proceedings of the Adaptive Structures and Material Systems Symposium—*2000 *ASME IMECE*, Vol. **60**, 285–297. An active–passive piezoelectric vibration absorber for structural control under harmonic excitations with time-varying frequency.
6. M. S. TSAI and K. W. WANG 1999 *Journal of Sound and Vibration* **221**, 1–22. On the structural damping characteristics of active piezoelectric actuators with passive shunt. doi:10.1006/jsvi.1998.1841.
7. J. H. HOLLKAMP 1994 *Journal of Intelligent Material Systems and Structures* **5**, 49–57. Multimodal passive vibration suppression with piezoelectric materials and passive electrical networks.
8. S. WU 1998 *Proceedings of the SPIE* **3327**, 159–168. Method for multiple mode shunt damping of structural vibration using a single PZT transducer.
9. P. HANDEL and P. TICHAVSKY 1994 *International Journal of Adaptive Control and Signal Processing* **8**, 447–456. Adaptive estimation for periodic signal enhancement and tracking.
10. C. T. CHEN 1984 *Linear System Theory and Design*, 413 New York: Holt, Rinehart and Winston, Inc.
11. H. K. KAHLIL 1996 *Nonlinear Systems*, 100. Englewood Cliffs, NJ: Prentice-Hall.
12. C. R. FULLER, S. J. ELLIOTT and P. A. NELSON 1996 *Active Control of Vibration*, 91–113. London: Academic Press.